Design of a Superconducting Magnet for Lorentz Force Electrical Impedance Tomography (LFEIT)

Boyang Shen, *Student Member*, *IEEE*, Lin Fu, Jianzhao Geng, Heng Zhang, Xiuchang Zhang, Zhaoyang Zhong, Zhen Huang, and T. A. Coombs

***Abstract*—This paper presents the design and modeling of a Second Generation (2G) High Temperature Superconducting (HTS) magnet which is suitable for Lorentz Force Electrical Impedance Tomography (LFEIT). The concept of constructing superconducting magnet using the configuration of Halbach Array is proposed, which can achieve a favorable thin geometry for LFEIT system, and is able to build a homogenous magnetic field with high intensity. The modeling of this superconducting Halbach Array magnet has been executed by COMSOL Multiphysics. *H*-formulation together with *B*-dependent critical current density and bulk approximation are used as the basic tools for modeling. Results reveal this magnet can achieve over 1 Tesla magnetic field in the cross-section required. The optimization of HTS coils' location and different numbers of coils are carried out to balance the strength and homogeneity of magnetic field.**

***Index Terms*—Superconducting magnet, Lorentz Force Electrical Impedance Tomography (LFEIT), Halbach Array, HTS coil.**

I. Introduction

Since last century, the research on electrical impedance of human tissues has become tremendously popular all over the world [1]. The technologies to image the electrical impedance of biological tissues can make great contribution to the early diagnosis of cancer and stroke [2]. Lorentz Force Electrical Impedance Tomography (LFEIT) is a novel and promising configuration for diagnostic scanner which is able to achieve the 3D high resolution imaging of tissue impedance based on ultrasonically induced Lorentz force [3].

The working principle of LFEIT is to image the electrical signal generated by the magneto-acoustic effect from a biological sample [3]. As shown in Fig. 1, a sample is located in a magnetic field (z direction) and an ultrasound wave (y direction) propagates through its conductive medium [4]. The ultrasound propagation causes the free ions and charges in the biological tissue moving within the magnetic field, which can generate the magneto-acoustic to induce a Lorentz current flow within the tissue [5]. LFEIT has several advantages over conventional electrical impedance tomography and other medical imaging techniques, e.g. excellent bio-detection of soft tissues, high spatial resolution, portability for emergency diagnosis (could potentially be equipped into an ambulance) and relatively low manufactory cost [4], [5].

The authors are with the Electrical Engineering Division, Department of Engineering, University of Cambridge, CB3 0FA, U.K. (e-mail: bs506@cam.ac.uk).

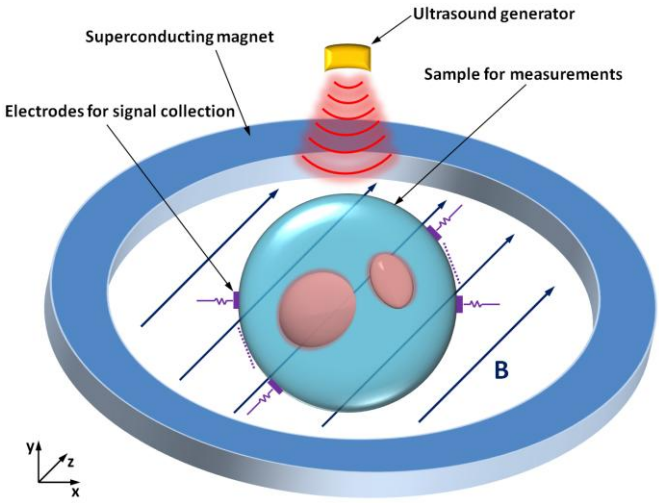

Fig. 1. Configuration of superconducting Lorentz Force Electrical Impedance Tomography (LFEIT).

For LFEIT system, magnet is a crucial component. The intensity of magnetic field directly affects the imaging quality of biological tissues. For a small scale experimental LFEIT system, permanent magnet could be used to create an appropriate field [4]. However, for a large diagnostic LFEIT system like a whole body scanner which requires intensity more than 1 Tesla, permanent magnets are not able to realize the portability for LFEIT system due to their heavy weight and large geometry [6].

Therefore, we tried to use the combination of superconducting magnet with LFEIT system. A compact superconducting magnet can produce a homogenous magnetic field with high intensity, which could be significantly beneficial for the enhancement of electrical signal output and the robustness to noise, especially for the large scale LFEIT system [7]. Fig. 1 demonstrates the configuration of superconducting LFEIT, which covers a superconducting magnet, an ultrasound generator and a signal collection system.

As the most favorable structure utilized for MRI, superconducting Helmholtz Pair magnet is capable for providing a magnetic field with proper strength and extremely good homogeneity [8]. But Helmholtz Pair occupies a large space due to specific arrangement for Helmholtz coils location, namely, the coils' radius *R* equal to the axial distance of two coils *D* is needed to create uniform magnetic field,

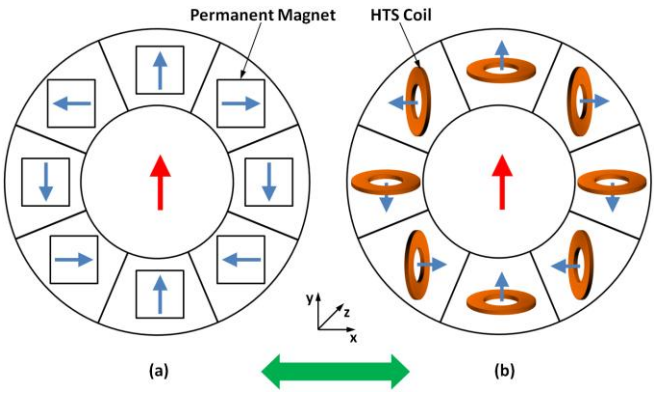

Fig. 2. (a) Configuration of permanent magnet based Halbach Array magnet. (b) Configuration of HTS coils based Halbach Array magnet.

which could bring difficulties of huge magnet size. Halbach Array is an effective arrangement of magnets that is able to generate a homogenous magnetic field [9], whose geometry has thin depth in z direction in Fig. 2. A practical Halbach magnet was tested experimentally to generate a uniform field for a Lorentz-force hydrophone [10]. Therefore, a reasonable idea is sparked: it could use superconducting coils to build an electromagnet that operating below its critical temperature, which is essentially equivalent to the Halbach Array based on permanent magnets. This concept of superconducting Halbach Array magnet is presented in Fig. 2.

To the best of our knowledge, there is no research on design and simulation of superconducting magnet using the Halbach Array structure with High Temperature Superconducting (HTS) coils, especially for LFEIT system. This paper demonstrates the modeling of superconducting Halbach Array magnet using the FEM software COMSOL Multiphysics. The target of this conceptual magnet design is to achieve average magnetic strength over 1 Tesla and acceptable inhomogeneity ($(B_{max}$-$B_{min})/B_{average}$) less than 100 ppk (parts per thousand) within 60 cm diameter circular cross-section for a potential full-body LFEIT system.

II. Design and Modeling for Superconducting Halbach Array Magnet

A. 2D *H*-formulation

H-formulation is one of the most popular methods to realize superconducting modeling, which calculates the solution of the induced current and magnetic field distribution under the framework of the Maxwell Ampere's Law (1), Faraday's Law (2), Constitutive Law (3), Ohm's Law (4) and *E*-*J* power law (5) [11]:

$$\nabla \times H = J \tag{1}$$

$$\nabla \times E = -\frac{\partial B}{\partial t} \tag{2}$$

$$B = \mu_0 \mu_r H \tag{3}$$

$$E = \rho J \tag{4}$$

$$E = E_0 \left(\frac{J}{J_c} \right)^n \tag{5}$$

Where $\boldsymbol{H}$ is the magnetic field intensity, $\boldsymbol{J}$ is the current density, $\boldsymbol{E}$ is the electric field, $\boldsymbol{B}$ is the magnetic flux density, μ_0 is the permeability of free space, μ_r is the relative permeability, ρ is the resistivity, E_0 is the characteristic electric field, J_c is the critical current density and n is the factor for *E*-*J* power law. Combining (1), (2), (3), (4) and (5), the general form of 2D partial differential equation (PDE) for dependent variables $\boldsymbol{H}$ is:

$$\mu_0 \mu_r \frac{\partial H}{\partial t} + \nabla \times \left(\rho \nabla \times H \right) = 0 \tag{6}$$

which can be solved by COMSOL Multiphysics.

B. Magnet Design and Modeling

The superconducting Halbach Array magnet was constructed on the basis of Halbach Array configuration with HTS coils. The modeling and simulation of this magnet was based on partial differential equations above. The HTS material for this design was simulated as the 1.2 cm wide YBCO tape manufactured by SuperPower® [12], with critical 300 A at 77 K. As shown in Fig. 2 (b), a superconducting Halbach Array magnet consists of eight HTS coils which were placed in the Halbach ring. The distances from the centre of each coil to the centre of Halbach ring were all identical to the distance D_c. These eight coils also carried the same amount of current and each coil had a 90 degree phase change to the next coil. The direction of magnetic field generated from each coil is shown in Fig. 2 (b).

The ***B***-dependent critical current model was also used for this design. J_c can be reduced in the parallel and perpendicular magnetic field [13]:

$$J_c(B) = \frac{J_0}{\left(1 + \sqrt{\frac{k^2 B_{para}^{\ 2} + B_{perp}^{\ 2}}{B_0}} \right)} \tag{7}$$

J_0 is the critical current in zero magnetic field, 77 K. The parameters used in (7) are k = 0.186 and B_0 = 0.426 presented in literature [13]. It can be found that the perpendicular component is significantly higher than the parallel component.

For this design, wound coil with layers of coated conductor was represented by continuous area bulk approximation in order to improve model convergence and simulation speed [13]. The transport current was injected into the HTS coils using the Pointwise constraint from general PDE model, which was able to force the integration of current density J_s within bulk approximation over cross-section area A equal to the magnitude of the transport current I_s in each tape multiplied by the number of turns N:

$$NI_s = \int J_s dA \tag{8}$$

Each bulk approximation had the cross-section of 4.8 cm width and 5 cm thickness, which was used to represent 2000 turns (4×500 turns of a single layer rectangular coil) YBCO coils for this design. As shown in Fig. 3, all the coils were fixed in the non-magnetic Halbach Array frame, and air was set in the ring circle. The DC current 120 A was applied to each tape using a ramp function to achieve an increment of full current in the first 0.2 s, and then remained this value. The specification of superconducting Halbach Array design is shown in TABLE I.

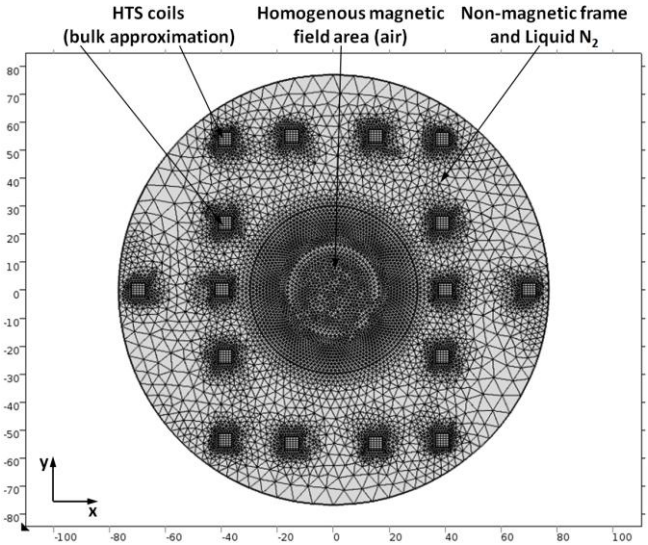

Fig. 3. Mesh for superconducting Halbach Array design.

TABLE I
SPECIFICATION FOR SUPERCONDUCTING HALBACH ARRAY MAGNET

Parameters	Value
Inner diameter	60 cm
Outer diameter	156 cm
D_c (distance from coils centre to ring centre)	55 cm
YBCO tape cross-section	1.2 cm × 0.01 cm
Bulk approximation cross-section	4.8 cm ×5 cm
μ_0	$4\pi\times10^{-7}$ H/m
n (E-J Power Law factor)	21
J_{c0}	10^8 A/m^2
E_0	10^{-4} V/m
I_{app}	120 A

Fig. 3 presents the mesh for the superconducting Halbach Array design. It can be seen that the map meshes with intensive density were applied in the superconducting regions. Extremely high density free triangular meshes were distributed in centre circle of Halbach Array, which is the most important part in this design. The remaining meshes were relatively incompact for non-magnetic frame and other parts of the model. The air region outside the Halbach array was set as a square with each boundary length 10 times greater than the diameter of Halbach array, which was hidden in Fig. 3 for the purpose of presenting more details of this design.

Fig. 4 illustrates the centre of superconducting Halbach ring cross-section. It can be seen that the direction of magnetic flux inside the Halbach ring centre is almost in +y direction (the red arrow in Fig. 4). According to the contour plot in Fig. 4 for the magnetic flux density of Halbach ring centre cross-section, the flux density is around 1.0 T to 1.2 T in the most part of the ring, but there are still two high-intensity areas in the end of the radius along x-axis, while some relative low fields appear near the top and bottom of y-axis.

III. OPTIMIZATION AND DISCUSSION

Some optimization can be carried out for the purpose of further improving the electromagnetic performance of superconducting Halbach array. In this section, the optimization on the coils location (D_c, the distances from each HTS coil centre to Halbach ring centre) and different numbers of HTS coils are presented according to the simulation data.

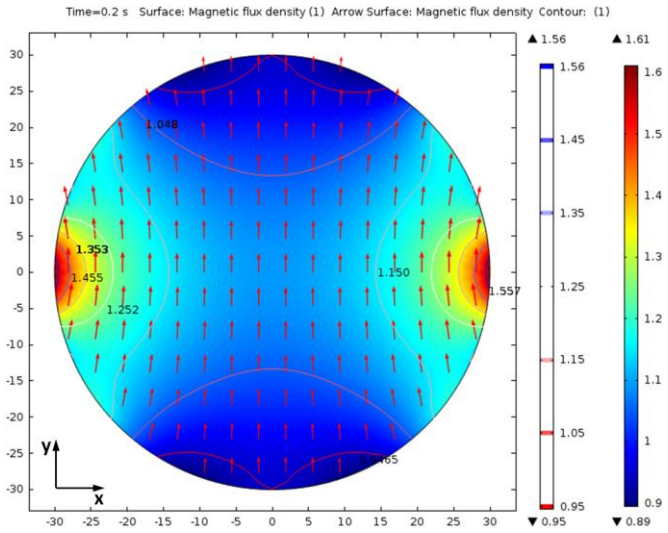

Fig. 4. Magnetic flux density (with direction and contour plot) in superconducting Halbach ring centre cross-section.

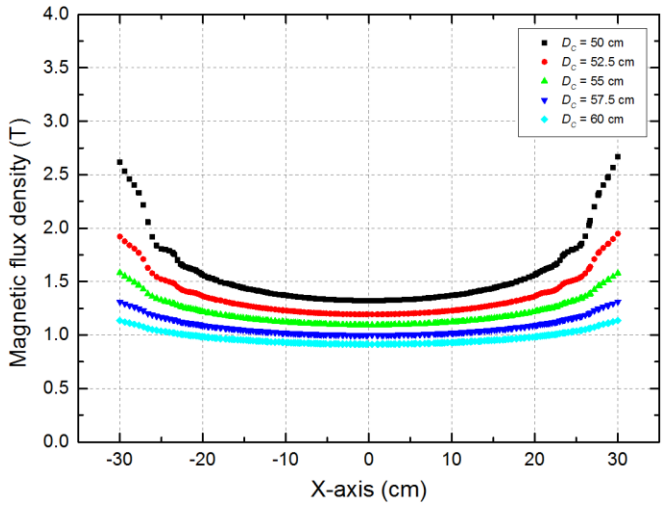

Fig. 5. Relationship between the magnetic flux density on diameter along x-axis and different D_c (five cases: D_c = 50, 52.5, 55, 57.5, 60 cm).

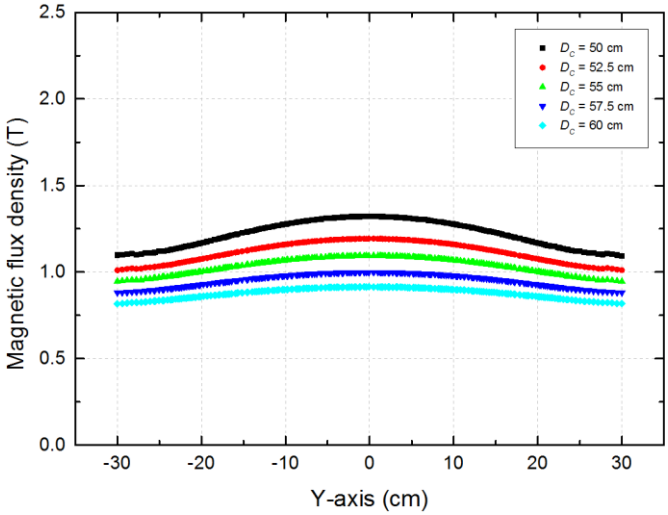

Fig. 6. Relationship between the magnetic flux density on diameter along y-axis and different D_c (five cases: D_c = 50, 52.5, 55, 57.5, 60 cm).

A. D_c Optimization

Fig. 5 presents the relationship between the magnetic flux density on the diameter of Halbach ring centre along x-axis

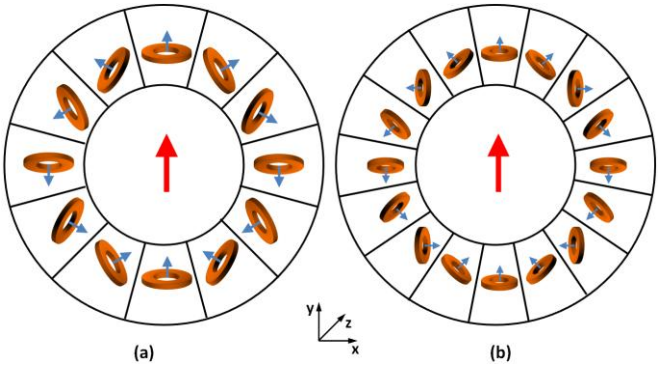

Fig. 7. Halbach arrangement for: (a) 12 HTS coils, (b) 16 HTS coils, with the same D_c as the 8 coils.

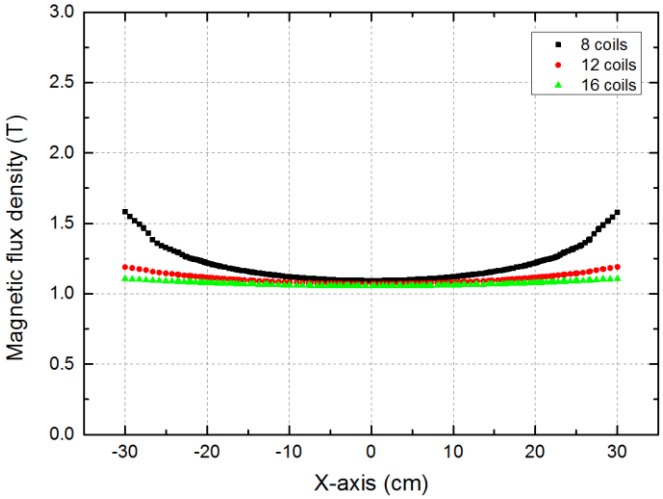

Fig. 8. Relationship between the magnetic flux density on diameter along x-axis and different numbers of coils (three cases: 8, 12 and 16 coils).

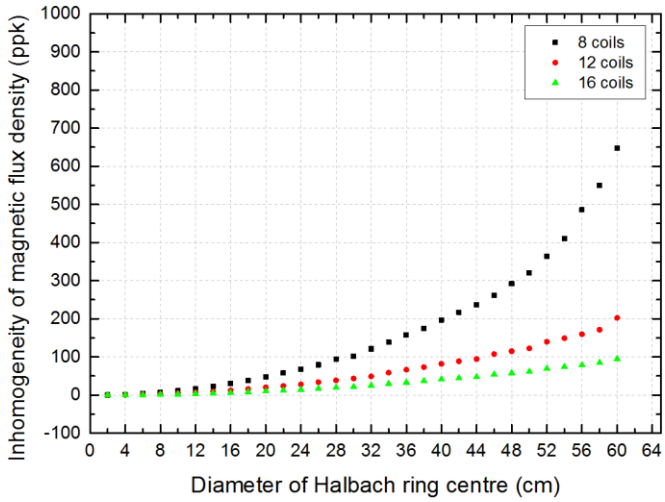

Fig. 9. Relationship between surface inhomogeneity of magnetic flux density in the Halbach ring centre cross-section and different numbers of coils (three cases: 8, 12 and 16 coils).

and different D_c, while Fig. 6 shows the relationship with y-axis. It can be found that for the cases of $D_c = 50$ cm and $D_c = 52.5$ cm, the magnetic flux density sharply rises and falls at the end of two sides of diameter along x-axis and y-axis, which is due to the HTS coils were placed too close to the Halbach ring centre. By contrast, there are only slightly decreasing and increasing trend of the flux density at the end of two sides when the D_c is greater than 52.5 cm. However, the magnetic flux density in most middle region along y-axis is below 1 T in the circumstances of $D_c = 57.5$ and 60 cm, which is lower than the target required.

B. Optimization for Numbers of Coils

Without changing the total amount of superconductor, optimization on using different numbers of coils for Halbach arrangement can be done by shrinking each coil's size with increasing number of coils. Fig. 7 reveals the Halbach arrangement for 12 coils (each coil has 60 degree phase change) and 16 coils (each coil has 45 degree phase change), which remains the same D_c = 55 cm as the 8 coils. Fig. 8 demonstrates the relationship between the magnetic flux density on diameter along x-axis and different numbers of coils. It can be seen that the magnetic field is all above 1 T for all these three cases, and it becomes more uniform when the coil's number increases from 8 to 16. To be more precise, Fig. 9 shows as relationship between surface inhomogeneity of magnetic flux density in the Halbach ring centre cross-section and different numbers of coils. The magnetic homogeneity has improved significantly with the increasing number of coils. With the 12 coils case, the inhomogeneity is lower than 100 ppk (parts per thousand) inside the circular region with 44 cm diameter of the centre cross-section. For the case of 16 coils, the inhomogeneity is below 100 ppk in the entire region of Halbach ring centre cross-section (60 cm diameter circular region), which is broadly in the acceptable region due to that 100 ppk inhomogeneity is sufficient because LFEIT does not require highly homogeneous magnetic field if the magnetic strength is around 1 T. Unlike MRI, LFEIT does not significantly rely on the magnetic field with extremely high homogeneity as LFEIT obtains the characteristic of ultrasound imaging which can realize accurate location of signals [4].

IV. Conclusion

An effective method to build superconducting magnet using Halbach Array configuration is proposed for LFEIT system. It can generate appropriate magnetic field within 60 cm diameter cross-section and use a thin geometry, which potentially enables LFEIT working for emergency diagnosis in an ambulance. A 2D model of superconducting Halbach Array magnet has been developed using ***H***-formulation based on ***B***-dependent critical current density and bulk approximation, with the FEM platform of COMSOL Multiphysics. Their magnetic properties such as magnitude, direction and homogeneity of magnetic field have been analyzed and the results show the magnet works as expected. The optimized case of 16 HTS coils with D_c = 55 cm can realize the magnetic flux density over 1 T with acceptable magnetic inhomogeneity less than 100 ppk in the entire 60 cm diameter region of Halbach ring centre cross-section. Without changing the total amount of superconductor, optimization results show that magnetic homogeneity can be efficiently improved by increasing the number of coils for Halbach arrangement while shrinking each coil's size.

V. References

[1] C. Gabriel, S. Gabriel, and E. Corthout, "The dielectric properties of biological tissues: I. Literature survey," *Phys. Med. Biol.*, vol. 41, no. 11, pp. 2231, 1996.

[2] Y. Zou, and Z. Guo, "A review of electrical impedance techniques for breast cancer detection," *Med. Eng. & Phys.*, vol. 25, no. 2, pp. 79-90, 2003.
[3] H. Wen, J. Shah, and R. S. Balaban, "Hall effect imaging," *IEEE Trans. Biomed. Eng.*, vol. 45, no. 1, pp. 119-124, 1998.
[4] P. Grasland-Mongrain, J. Mari, J. Chapelon, and C. Lafon, "Lorentz force electrical impedance tomography," *IRBM*, vol. 34, no. 4, pp. 357-360, 2013.
[5] S. Haider, A. Hrbek, and Y. Xu, "Magneto-acousto-electrical tomography: a potential method for imaging current density and electrical impedance," *Physiol. Meas.*, vol. 29, no. 6, pp. S41, 2008.
[6] J. Gieras, *Permanent magnet motor technology: design and applications*: CRC press, 2002.
[7] T. Coombs, Z. Hong, Y. Yan, and C. Rawlings, "The next generation of superconducting permanent magnets: The flux pumping method," *IEEE Trans. Appl. Supercond.*, vol. 19, no. 3, pp. 2169-2173, 2009.
[8] S. Lin, and A. Kaufmann, "Helmholtz coils for production of powerful and uniform fields and gradients," *Rev. Mod. Phys.*, vol. 25, no. 1, pp. 182, 1953.
[9] K. Halbach, "Design of permanent multipole magnets with oriented rare earth cobalt material," *Nucl. Instrum. Methods.*, vol. 169, no. 1, pp. 1-10, 1980.
[10] P. Grasland-Mongrain, J. Mari, B. Gilles, A. Poizat, J. Chapelon, and C. Lafon, "Lorentz-force hydrophone characterization," *IEEE Trans. Ultrason., Ferroelect., Freq. Control*, vol. 61, no. 2, pp. 353-363, 2014.
[11] Z. Hong, A. Campbell, and T. Coombs, "Numerical solution of critical state in superconductivity by finite element software," *Supercond. Sci. Technol.*, vol. 19, no. 12, pp. 1246, 2006.
[12] SuperPower, "SuperPower® 2G HTS Wire Specifications," Schenectady, NY 12304, USA.
[13] M. Ainslie, Y. Jiang, W. Xian, Z. Hong, W. Yuan, R. Pei, T. Flack, and T. Coombs, "Numerical analysis and finite element modelling of an HTS synchronous motor," *Physica C*, vol. 470, no. 20, pp. 1752-1755, 2010.